

2195 铝锂合金 T 型接头双侧激光摆动焊接组织与性能分析

雷正龙^{1*}, 毕思源¹, 张新瑞¹, 黎炳蔚¹, 夏佩云²

¹ 哈尔滨工业大学先进焊接与连接国家重点实验室, 黑龙江 哈尔滨 150001;

² 上海航天设备制造总厂有限公司, 上海 200245

摘要 2195-T87 铝锂合金是轻质高强的新一代航空材料, 但相比于传统铝合金, 铝锂合金的焊接难度更高。基于铝锂合金蒙皮-桁条结构的焊接需求, 采用激光束圆形摆动的方式配合 Al-Si 焊丝对 2195-T87 铝锂合金 T 型接头进行双侧激光摆动焊接, 对比摆动激光焊接与无摆动激光焊接所得接头的焊缝成形与组织特征, 并探讨了热输入、摆动频率以及摆动幅度对焊缝成形质量的影响, 最终获得了优化工艺参数下的接头横向与轴向拉伸强度, 分析了通过光束摆动改善焊缝成形质量、提高接头强度的效果。结果表明, 采用高焊速、低热输入与中等摆动幅度和摆动频率的双侧激光摆动焊接可改善焊缝表面成形质量, 抑制气孔生成, 细化焊缝晶粒, 缩小等轴细晶区尺寸, 进而提高接头的横向与轴向拉伸性能, 所得接头的最大轴向拉伸强度为 267 MPa, 横向拉伸强度为 420 MPa, 对比无摆动焊接分别提高了 123 MPa 和 95 MPa, 达到了母材强度的 45% 和 70%。

关键词 激光技术; 铝锂合金 T 型接头; 双侧激光摆动焊接; 显微组织; 力学性能

中图分类号 TG457.14 文献标志码 A

doi: 10.3788/CJL202249.0802003

1 引言

航空航天制造业作为现代制造业的“皇冠”, 集成了大量的现代高新技术, 而对飞行器进行轻量化的制造与加工一直以来都是航空航天制造业领域的发展热点之一。2195 铝锂合金是一种典型的第三代铝锂合金, 有着质量轻、强度高且低温力学性能和抗蚀性能优越等优点, 十分契合航空航天工业的发展要求^[1-4]。美国洛马公司生产的超轻型航天飞机燃油贮箱, 将 2219 铝铜合金替换为 2195 铝锂合金, 在维持原强度的同时整体减重高达 3405 kg^[5]。

对高强度铝锂合金蒙皮-桁条 T 型结构的连接以铆接为主, 结构质量重, 难以实现轻量化^[6-7]。激光焊接的热输入集中, 热影响区窄, 焊接应力低, 焊接变形小, 常用于铝合金的焊接^[8]。双侧激光焊接技术相较于铆接技术, 连接结构质量更轻、工作效率更高, 有着取代传统铆接技术的潜力^[9]。目前, 该技

术在空客 A340、A350 等型号飞机生产制造上已得到应用, 在维持原本结构刚度的前提下, 结构质量下降幅度可达 20%, 生产成本降幅可达 25%^[10]。然而, 锂(Li)的加入使得铝锂合金相较传统铝合金有着更高的焊接气孔与热裂纹敏感性, 采用激光对新型铝锂合金进行焊接的难度远高于焊接传统中等强度的铝合金^[11-12]。激光摆动焊接让激光光束根据预先设计的轨迹一边焊接一边摆动, 对熔池产生搅拌作用, 促进合金元素均匀化, 获得晶粒度更小的组织, 从而改善接头的力学性能, 能够抑制焊接缺陷的形成, 提高焊缝质量^[13-17]。对 2 mm 厚 2060 铝锂合金对接接头的激光摆动焊接工艺的研究表明, 光束摆动促进熔池流动, 减小了焊丝引入的熔融金属对匙孔的冲击作用, 可维持焊接匙孔稳定存在, 为熔池中气泡逸出提供充足时间, 有效抑制焊缝气孔生成, 且光束摆动的搅拌作用可细化晶粒, 显著提升接头的拉伸强度^[18-19]。

收稿日期: 2021-07-26; 修回日期: 2021-08-17; 录用日期: 2021-08-24

基金项目: 国家科技重大专项(2019ZX04025001)

通信作者: *leizhenglong@hit.edu.cn

目前对铝锂合金T型接头双侧激光焊接的研究主要集中在通过调整工艺参数或改进焊丝化学组分来提高焊接质量,但主要针对2 mm以下薄板,对由4~6 mm较厚板材组成的T型接头的焊接以及双侧激光摆动焊接的研究较少。本文采用光纤激光器对2195铝锂合金T型接头进行双侧激光焊接,对比摆动与无摆动焊接的焊缝成形、组织特征以及横向和轴向拉伸性能,得出通过光束摆动来改善焊缝成形、提高接头强度的机理,为2195铝锂合金T型接头双侧激光摆动焊接的工程应用提供参考。

表1 2195铝锂合金的化学成分及含量

Table 1 Main chemical composition and content of 2195 Al-Li alloys

Element	Li	Cu	Mg	Zr	Ag	Fe	Mn	Si	Al
Mass fraction /%	1.0	4.0	0.38	0.13	0.35	0.12	0.01	0.12	Bal.

表2 ER4047焊丝的化学成分及含量

Table 2 Main chemical composition and content of ER4047 welding wire

Element	Si	Fe	Cu	Mn	Zn	Ti	Mg	Al
Mass fraction /%	11.52	0.20	<0.001	0.01	0.001	0.01	0.01	Bal.

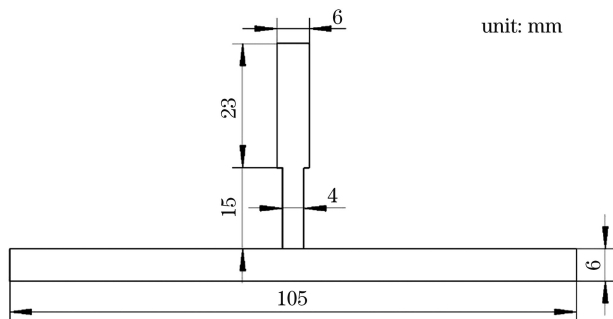


图1 蒙皮-桁条T型接头结构尺寸

Fig. 1 Size of the skin-stringer T-joint

试验所用的激光焊接系统由两台YLS 6000光纤激光器、两台KUKA焊接机器人和龙门行走机构、焊接专用工作台等部分组成。激光器的最大输出功率为6 kW,波长为1.06 μm,最小光斑直径为0.26 mm。采用FRONIUS的送丝系统,送丝速度

2 试验材料及方法

本试验采用的蒙皮和桁条材料均为2195-T87铝锂合金,平均拉伸强度为598 MPa,填充材料为1.2 mm直径的ER4047铝合金焊丝,主要化学成分和含量见表1和表2。蒙皮厚度为6 mm,桁条截面为凸台状截面,底部厚度为4 mm,上部厚度为6 mm,桁条和蒙皮共同组成T型接头,尺寸如图1所示。本试验中T型结构构件的尺寸为400 mm×105 mm,包括1根桁条。焊前及时去除母材表面的氧化膜。

表1 2195铝锂合金的化学成分及含量

Table 1 Main chemical composition and content of 2195 Al-Li alloys

在0.03~9.99 m/min范围内精确可调,以保证焊丝匀速平稳地送达焊接位置。采用填丝双侧激光焊接方法,送丝速度 $v'=4$ m/min,摆动方式选用圆形摆动,激光束运动路径如图2所示,光束入射角为30°,激光束、保护气喷嘴和焊丝位于同一平面内。焊接过程中采用前送丝的方式送丝。保护气体为Ar/He混合气,气流量为15~20 L/min;试验过程如图3所示,送丝设备在前,送气设备在后。

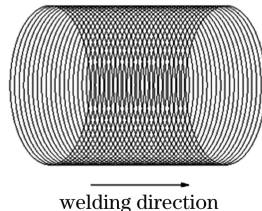


图2 圆形摆动激光束的运动路径

Fig. 2 Movement path of circular swinging laser beam

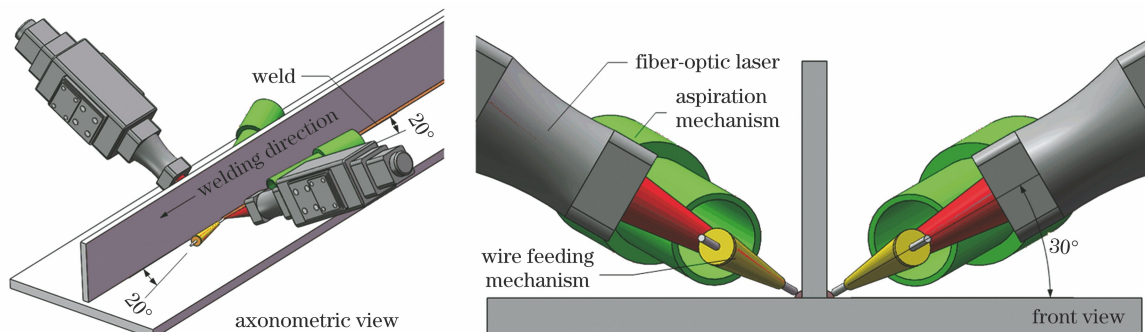


图3 双侧激光焊接过程示意图

Fig. 3 Schematic of double-sided laser welding process

焊接完成后,通过线切割的方法把试样从焊接试件上截取出,采用牙托粉进行湿法镶样,用180#、400#、600#、1000#、1500#以及2000#砂纸磨光试样,之后进行抛光,洗净后使用凯勒试剂进行腐蚀,用VCM3000G-TV金相显微镜拍摄金相试样截面。使用HELIOS NanoLab 600i离子/电子双束系统-SEM/EDS扫描电镜进行组织拍

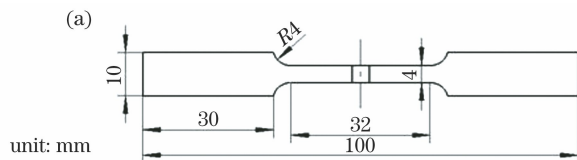


图4 横向拉伸试件尺寸及加载方向。(a)试样尺寸;(b)加载方向

Fig. 4 Transverse tensile specimen size and loading direction. (a) Specimen size; (b) loading direction

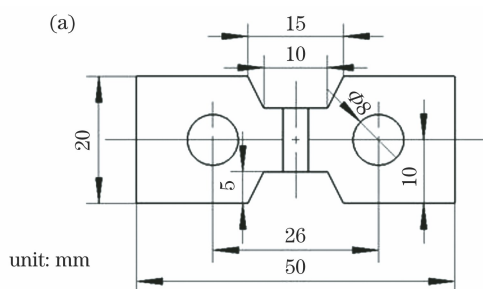
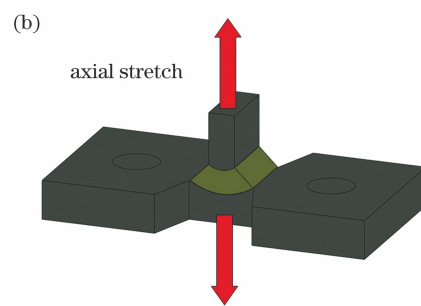


图4 横向拉伸试件尺寸及加载方向。(a)试样尺寸;(b)加载方向

Fig. 4 Transverse tensile specimen size and loading direction. (a) Specimen size; (b) loading direction



3 分析与讨论

3.1 摆动激光焊接特性

图6和图7分别对比了同时采用4000 W激光功率,3 m/min焊接速度,4 m/min送丝速度的工艺参数时无摆动焊接与摆动焊接所得T型接头的侧面与横截面形貌,其中摆动焊接的摆动方式为圆形摆动,摆动幅度为0.8 mm,摆动频率为200 Hz。可见摆动焊接所得焊缝表面成形相比无摆动焊接更加饱满均匀,且无摆动焊接所得接头横截面气孔数

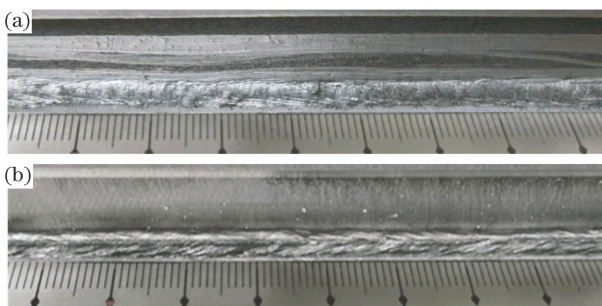
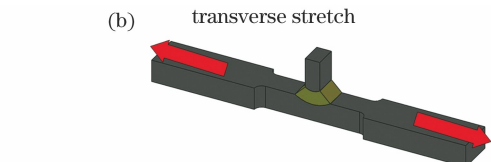


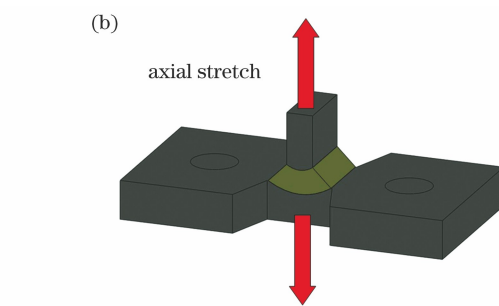
图6 焊缝侧面形貌。(a)无摆动激光焊接;(b)摆动激光焊接

Fig. 6 Profile morphologies of weld. (a) Laser welding without swing; (b) laser welding with swing

摄,不对拍摄用试样进行腐蚀。在电子万能试验机AGX-plus250kN上进行拉伸性能测试,拉伸方式包括横向拉伸(沿蒙皮方向进行拉伸)和轴向拉伸(沿桁条方向进行拉伸)两种,加载速度为2 mm/min,两种拉伸试样的尺寸与加载方向分别如图4和图5所示,其中轴向拉伸采用专门的拉伸夹具。



(b) transverse stretch



(b)

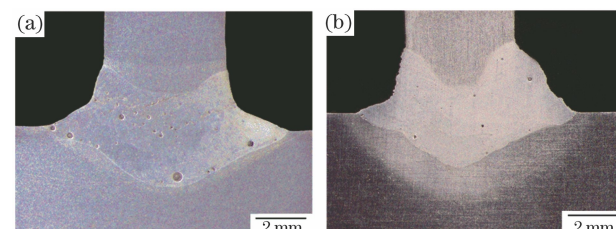


图7 接头横截面形貌。(a)无摆动激光焊接;(b)摆动激光焊接

Fig. 7 Cross-sectional morphologies of joint. (a) Laser welding without swing; (b) laser welding with swing

量更多,这是因为摆动焊接通过光束摆动的搅拌作用加速了熔池流动,焊丝引入的熔融金属在匙孔侧壁产生的凸起幅度受匙孔高速流动的影响而减小,从而缓解了焊丝熔入对匙孔的冲击作用,匙孔更加稳定不易塌陷,且熔池流动带动更多气体向外逸出,抑制了气孔的形成,改善了焊缝成形状况^[18]。

分别在焊缝中部截取100 mm对无摆动焊接与摆动焊接试样进行射线探伤,所得底片如图8所示。无摆动焊接所得焊缝内部气孔数量显著多于摆动焊接,且气孔尺寸更大,分布更为密集。可见摆动焊接对气孔缺陷有更好的抑制作用,统计结果表明,摆动激光焊接使气孔率从无摆动的1.89%

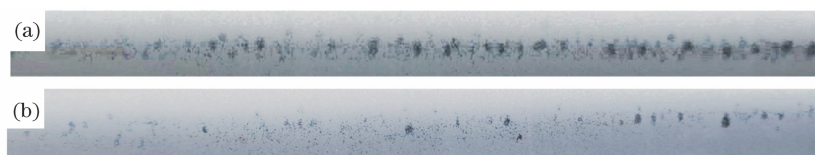


图8 焊接试样射线探伤底片。(a)无摆动激光焊接;(b)摆动激光焊接

Fig. 8 Negative films of radiographic flaw detection of welded samples. (a) Laser welding without swing; (b) laser welding with swing

降低至0.5%。

3.2 焊接工艺参数对接头宏观形貌的影响

表3列出了3种热输入下双侧激光摆动焊接所得T型接头的宏观形貌,其中摆动幅度均为0.8 mm,摆动频率均为200 Hz。随着焊接速度提

高与热输入降低,焊缝的波纹逐渐变得细致均匀,焊缝成形质量提升,熔深、熔宽逐渐减小,对蒙皮的热影响降低,且焊速较低的试样1和试样2在焊缝表面与横截面出现气孔。对比可见,采用高焊速、低热输入的工艺参数得到的接头成形质量较好。

表3 不同热输入下的双侧激光摆动焊接T型接头宏观形貌

Table 3 Macro morphology of double-sided laser swing welding T-joint under different heat inputs

Sample No.	Process parameter	Side morphology	Cross-sectional morphology
1	$v=1 \text{ m/min}$		
	$P=2800 \text{ W}$ $Q=1680 \text{ J/cm}$		
2	$v=2 \text{ m/min}$		
	$P=3300 \text{ W}$ $Q=990 \text{ J/cm}$		
3	$v=3 \text{ m/min}$		
	$P=4000 \text{ W}$ $Q=800 \text{ J/cm}$		

采用激光功率为4000 W,焊接速度为3 m/min,送丝速度为4 m/min的工艺参数,在不同摆动幅度与摆动频率下进行双侧激光摆动焊接,所得T型接头的宏观形貌分别如表4和表5所示。对比可见:随着摆动幅度与摆动频率的增大,焊缝表面波纹均变得更加细密,表面成形更为良好;摆动幅

度和摆动频率较低时,焊缝表面与横截面存在气孔,但在较高的摆动幅度和摆动频率下焊缝表面下塌更为明显,且摆动幅度过大会使有效热输入降低,从而导致壁板未完全熔透,如表4中试样6所示。综上所述,采用中等的摆动幅度与摆动频率可得到成形质量较好的接头。

表4 当摆动频率为200 Hz时,不同摆动幅度下的双侧激光摆动焊接T型接头宏观形貌

Table 4 Macro morphology of double-sided laser swing welding T-joint under different swing amplitudes when the swing frequency is 200 Hz

Sample No.	Swing amplitude / mm	Side morphology	Cross-sectional morphology
4	0.6		
5	0.8		
6	1.0		

表5 当摆动幅度为0.8 mm时,不同摆动频率下的双侧激光摆动焊接T型接头宏观形貌

Table 5 Macro morphology of double-sided laser swing welding T-joint under different swing frequencies when the swing amplitude is 0.8 mm

Sample No.	Swing frequency / Hz	Side morphology	Cross-sectional morphology
7	100		
8	200		
9	300		

3.3 接头微观组织

2195-T87铝锂合金T型接头双侧激光焊接接头组织如图9所示。根据组织特征的不同,可将接头分成4个区域,如图9(b)、(e)所示,从蒙皮到焊缝依次分为母材(BM)、热影响区(HAZ)、等轴细晶区(EQZ)和焊缝区(FZ),且桁条一侧的组织特征分区与蒙皮一侧相同。其中HAZ晶粒粗大,方向与母材轧制方向相同,如图9(f)所示;EQZ区域出现细小的等

轴晶粒,是熔合线处新晶粒非均匀形核长大的结果,如图9(b)、(e)所示;焊缝靠近熔合线区域向焊缝中心产生平行的柱状晶组织,如图9(c)所示。这是因为临近母材处有着大的热导率和低的结晶速率,结晶逐渐向熔池中心推进;当晶粒生长继续向熔池中心推进时,液相内部产生新的晶核,焊缝中部的晶核处于同种状态下,向各个方向的生长不受限制,从而形成了焊缝中间区域的等轴树枝晶,如图9(d)所示。

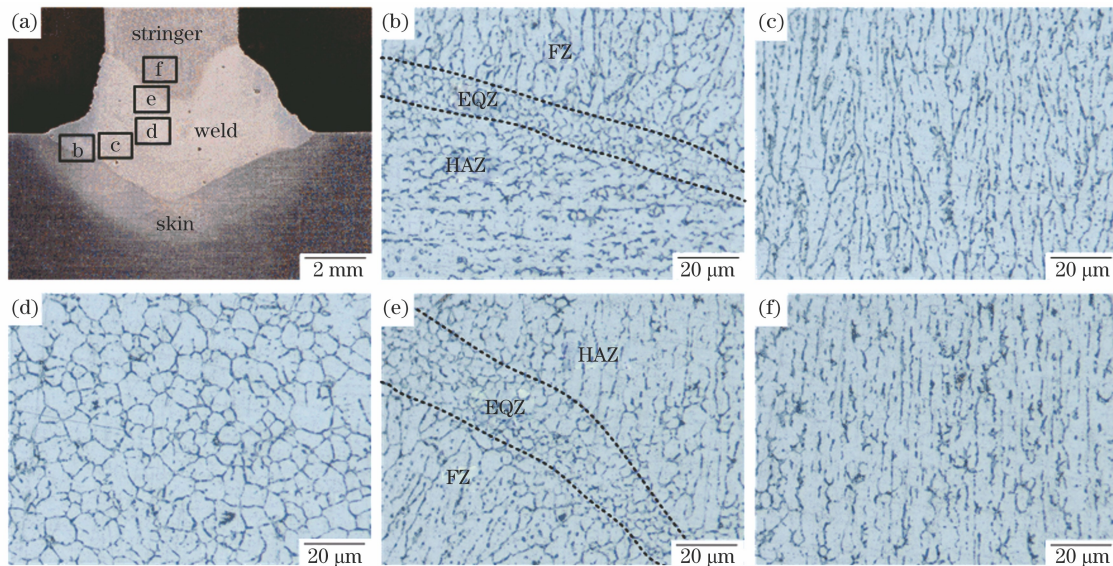


图9 2195铝锂合金双侧激光摆动焊接T型接头组织。(a)焊接接头宏观形貌;(b)~(e)熔合线、柱状晶区及中部等轴晶区;(f)热影响区

Fig. 9 Double-sided laser swing welding T-joint structure of 2195 Al-Li alloys. (a) Macro morphology of welded joint; (b)–(e) fusion line, columnar crystal area, and central equiaxed crystal area; (f) heat affected zone

焊缝中部等轴晶区的组织对比如图10所示。可以看到,摆动焊接的焊缝晶粒相较于无摆动焊接得到了显著细化,无摆动焊接获得的焊缝中部等轴晶平均直径约21 μm,而摆动焊接获得的焊缝中部等轴晶平均直径约13 μm,小于无摆动焊接所得晶

粒。激光束的摆动加速了熔池流动,使熔池中液态金属对已生长的柱状晶产生冲刷作用,破坏平行枝晶,部分已凝固的金属发生重熔,作为异质形核的质点,提高了形核率,晶粒尺寸由此得到细化^[19–20],从而增大了晶界面积,阻碍了裂纹扩展,使合金更容易

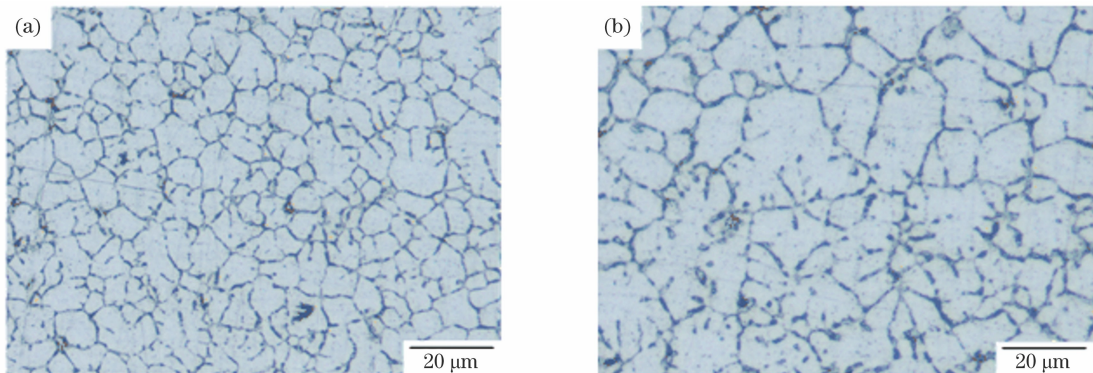


图 10 焊缝中部等轴晶区组织特征。(a)摆动激光焊接;(b)无摆动激光焊接

Fig. 10 Microstructure characteristics of equiaxed crystal zone in the middle of weld. (a) Laser welding with swing;
(b) laser welding without swing

适应细微处的应变,起到细晶强化的作用,提高了接头的承载能力。

摆动与无摆动焊接熔合区组织的对比如图 11 所示。在无摆动焊接接头的熔合区附近等轴细晶区宽约 $44 \mu\text{m}$,而在摆动焊接接头的熔合区附近等轴细晶区宽约 $23 \mu\text{m}$,尺寸明显减小。激光束的摆动

加速了熔池流动,抑制了熔池边缘第二相粒子的聚集,减小了层流边界层的厚度,进而缩小了等轴细晶区尺寸。等轴细晶区作为热裂纹敏感区域,其内部合金元素分布不均匀,易产生微裂纹^[21],缩小其尺寸可减少该区域内微裂纹数量,提高接头的承载能力。

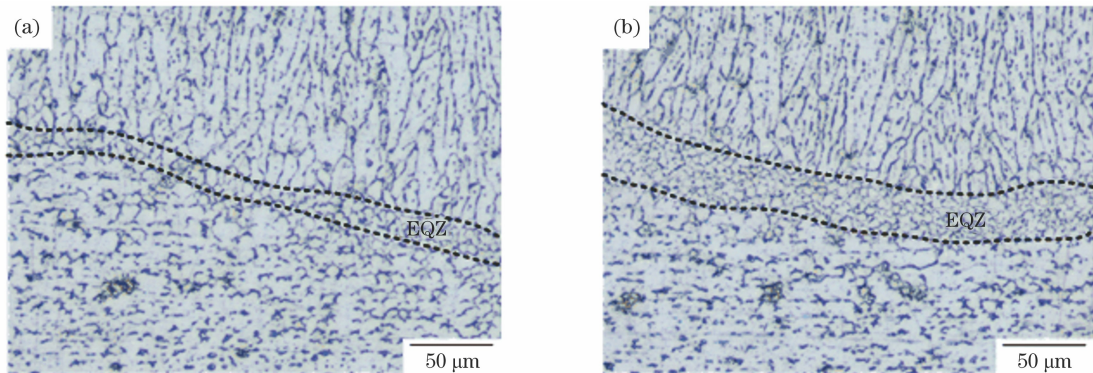


图 11 等轴细晶区组织特征。(a)摆动激光焊接;(b)无摆动激光焊接

Fig. 11 Microstructure characteristics of equiaxed fine-grained zone. (a) Laser welding with swing; (b) laser welding without swing

3.4 接头拉伸性能

采用前文优化后的工艺参数获得的双侧激光摆动焊接与无摆动焊接接头的横向与轴向拉伸性能对比如图 12 所示,可见摆动焊接接头的最大轴向拉伸强度约 267 MPa ,横向拉伸强度约 420 MPa ,比无摆动焊接分别提高了 123 MPa 和 95 MPa ,达到了母材强度的 45% 和 70% 。

摆动焊接轴向拉伸试样断裂发生在临近上熔合线的焊缝上部,断口形貌如图 13 所示,表面同时具有沿晶断裂与穿晶断裂的特征,韧窝间出现较明显的撕裂棱,部分韧窝底部存在第二相粒子分布,断裂机制为微孔聚集型断裂,兼具韧性断裂与脆性断裂的特点。摆动焊接横向拉伸试样的断裂从焊趾处开始,沿临近下熔合线的焊缝下部扩展并在最低点进

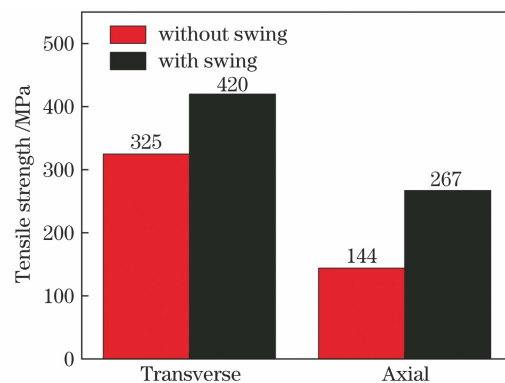


图 12 焊接接头拉伸强度对比

Fig. 12 Comparison of tensile strength of welded joint

入母材发生断裂,断口形貌如图 14 所示,其焊缝侧断口形貌与轴向拉伸断口相似,为微孔聚集型断裂,发生较大塑性变形,母材侧断口呈晶粒状,断裂机制

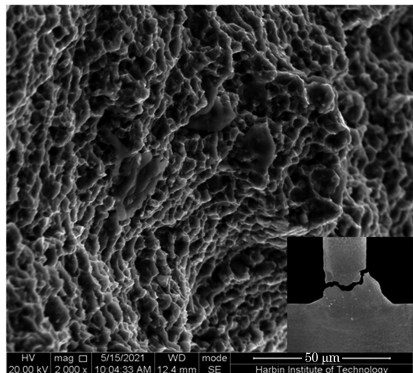


图 13 双侧激光摆动焊接轴向拉伸断口

Fig. 13 Axial tensile fracture of double-sided laser swing welding

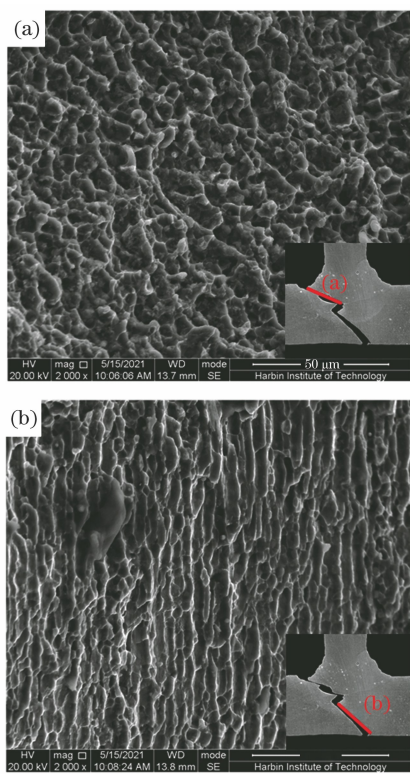


图 14 双侧激光摆动焊接横向拉伸断口。(a)焊缝侧断口;(b)母材侧断口

Fig. 14 Transverse tensile fracture of double-sided laser swing welding. (a) Weld side fracture; (b) base material side fracture

表现为准解理断裂和微孔聚集型断裂的复合。

4 结 论

采用圆形摆动方式进行双侧激光摆动焊接,获得了表面成形良好且气孔率低的 2195-T87 铝锂合金 T 型接头,其焊缝成形质量与气孔率优于相同工艺参数下的无摆动焊接接头,气孔率由 1.89% 降低至 0.52%。与常规双侧激光焊接相比,采用双侧激

光摆动焊接可通过光束摆动搅拌熔池,使焊缝中部等轴晶区晶粒得到明显细化,等轴细晶区尺寸显著缩小,从而提高了接头的承载能力,其中中部等轴晶的平均直径由 21 μm 下降至 13 μm ,等轴细晶区的平均宽度由 44 μm 下降至 23 μm 。双侧激光摆动焊接接头的最大轴向拉伸强度可达 267 MPa,横向拉伸强度可达 420 MPa,对比无摆动焊接分别提高了 123 MPa 和 95 MPa,达到了母材强度的 45% 和 70%。轴向拉伸和横向拉伸焊缝侧断口主要表现为微孔聚集型断裂,同时具有沿晶断裂和穿晶断裂的特征,横向拉伸母材侧断口表现为准解理断裂和微孔聚集型断裂的复合。

参 考 文 献

- [1] Xia L, Kang Y, Yu H S, et al. Equiaxed grains in laser welded 2060 Al-Li alloys and their formation mechanism[J]. Chinese Journal of Lasers, 2018, 45(11): 1102013.
- [2] Jiao S K, Liu S Y, Liu D, et al. Heat treatment microstructures and T_B phase precipitation of laser additive manufactured Al-Li alloys [J]. Chinese Journal of Lasers, 2018, 45(5): 0502001.
- [3] Ni B. Study on the laser weldability and welding technology of high strength aluminum-lithium alloy 2195[D]. Shanghai: Shanghai Jiao Tong University, 2016.
- [4] Mou H K, Huang X D, Yuan Y C, et al. Investigation of surface integrity of aluminum lithium alloy in high speed machining [J]. Scientia Sinica (Technologica), 2014, 44(1): 89-98.
- [5] Yu F S. Study on the weldability of 2195 Al-Li alloy of tank material for carrier rocket [D]. Tianjin: Tianjin University, 2018.
- [6] Mendez P F, Eagar T W. Welding process for aeronautics [J]. Advanced Materials and Processes, 2001, 159(5): 39-43.

- [7] Ryazantsev V I, Fedoseev V A, Matsnev V N. Technological aspects of assembly-welding all-welded passenger aircraft made of aluminium alloys [J]. Welding International, 2001, 15(1): 56-59.
- [8] Guo H T, Zhang D M, Zhao Y B, et al. Study on the formation of welding, microstructure, and properties of 5A06 aluminum alloy by ultrasonic laser-assisted filler welding [J]. Scientia Sinica (Technologica), 2020, 50(11): 1521-1528.
郭亨通, 张登明, 赵耀邦, 等. 5A06 铝合金超声辅助激光填丝焊接焊缝成形及组织性能研究[J]. 中国科学: 技术科学, 2020, 50(11): 1521-1528.
- [9] Liu T L, Zhang Y K, Dong P, et al. Mechanical property contrast research for laser beam welding and riveting of aluminum alloy joints [J]. Electromachining & Mould, 2019(S1): 56-58.
刘天亮, 张益坤, 董鹏, 等. 激光焊接与铆接铝合金接头力学性能对比研究[J]. 电加工与模具, 2019 (S1): 56-58.
- [10] Uz M V, Koçak M, Lemaitre F, et al. Improvement of damage tolerance of laser beam welded stiffened panels for airframes via local engineering [J]. International Journal of Fatigue, 2009, 31(5): 916-926.
- [11] Zhang X Y. Microstructures and mechanical properties of laser welded joints of 2060 aluminum lithium alloy [D]. Beijing: Beijing University of Technology, 2016.
张心怡. 2060 铝锂合金激光焊接组织及力学性能研究[D]. 北京: 北京工业大学, 2016.
- [12] Martukanitz R P, Jan R. A fundamental study of laser beam welding aluminum-lithium alloy 2195 for cryogenic tank application[R]. Washington, D. C.: NASA, 1996.
- [13] Shan Y, Du J J, Jiang H T, et al. Effect of beam scanning on microstructure of laser weld of 5A06 aluminum alloy [J]. New Technology & New Process, 2018(5): 40-43.
单莹, 杜俊杰, 蒋海涛, 等. 光束扫描对 5A06 铝合金激光焊缝组织的影响[J]. 新技术新工艺, 2018 (5): 40-43.
- [14] Liu H L, Zhou S W, Ma X Q, et al. Study on weld forming technology of laser swing welding on 6061 aluminum alloy sheet [J]. Mechanical & Electrical Engineering Technology, 2020, 49(2): 65-67, 133.
刘怀亮, 周邵巍, 马修泉, 等. 激光摆动焊接 6061 铝合金板材焊缝成形工艺研究[J]. 机电工程技术, 2020, 49(2): 65-67, 133.
- [15] Sun Q J, Li J Z, Liu Y B, et al. Formation, microstructure, and properties of electromagnetic field-assisted SUS316L austenite stainless steel laser narrow-gap joint [J]. Chinese Journal of Lasers, 2020, 47(10): 1002005.
孙清洁, 李军兆, 刘一搏, 等. 电磁场辅助 SUS316L 不锈钢扫描激光窄间隙焊接接头成形及组织性能[J]. 中国激光, 2020, 47(10): 1002005.
- [16] Wen P, Li Z X, Zhang S, et al. Investigation on porosity, microstructures and performances of 6A01-T5 aluminum alloy joint by oscillating fiber laser-CMT hybrid welding [J]. Chinese Journal of Lasers, 2020, 47(8): 0802003.
温鹏, 栗忠秀, 张松, 等. 摆动光纤激光-CMT 复合焊接 6A01-T5 铝合金型材接头的气孔特征及组织性能研究[J]. 中国激光, 2020, 47(8): 0802003.
- [17] Xu K X, Lei Z, Huang R S, et al. Effects of oscillation parameters on weld formation and porosity of titanium alloy narrow-gap laser wire filling welding [J]. Chinese Journal of Lasers, 2021, 48 (6): 0602111.
徐楷昕, 雷振, 黄瑞生, 等. 摆动工艺对钛合金窄间隙激光填丝焊缝成形及气孔率的影响[J]. 中国激光, 2021, 48(6): 0602111.
- [18] Chen G Y, Wang B, Zhong P X, et al. Laser scanning welding of 2060 Al-Li alloy with filler wire [J]. Transactions of the China Welding Institution, 2020, 41(4): 44-50, 99.
陈根余, 王彬, 钟沛新, 等. 2060 铝锂合金扫描填丝焊接工艺[J]. 焊接学报, 2020, 41(4): 44-50, 99.
- [19] Zhou X H, Zhao H Y, Liu F Y, et al. Effects of beam oscillation modes on microstructure and mechanical properties of laser welded 2060 Al-Li alloy joints[J]. Optics & Laser Technology, 2021, 144: 107389.
- [20] Bao G, Peng Y, Chen W Z, et al. Study on laser welding of ultra-fine grained steel with weaving beam [J]. Applied Laser, 2002, 22(2): 203-205, 208.
包刚, 彭云, 陈武柱, 等. 超细晶粒钢光束摆动激光焊接的研究[J]. 应用激光, 2002, 22(2): 203-205, 208.
- [21] Han B. Microstructure characteristics of double-sided laser beam welded aluminium lithium alloys T-joints and its crack control[D]. Harbin: Harbin Institute of Technology, 2018.
韩冰. 铝锂合金 T 型接头双侧激光焊接组织特征及裂纹控制研究[D]. 哈尔滨: 哈尔滨工业大学, 2018.

Microstructure and Mechanical Properties of Double-Sided Laser Swing Welding of 2195 Al-Li Alloy T-joints

Lei Zhenglong^{1*}, Bi Siyuan¹, Zhang Xinrui¹, Li Bingwei¹, Xia Peiyun²

¹ State Key Laboratory of Advanced Welding and Joining, Harbin Institute of Technology, Harbin, Heilongjiang 150001, China;

² Shanghai Aerospace Equipments and Manufacturer Co., Ltd., Shanghai 200245, China

Abstract

Objective 2195 aluminum-lithium compound is a typical third-generation aluminum-lithium alloy. It has the advantages of being lightweight and high strength, making it very suitable for usage in the aerospace industry. Laser welding has concentrated heat input and minor welding distortion. Compared with traditional riveting technology, double-sided laser welding technology has the advantages of lower connection structure weight and higher work efficiency. However, Li's addition makes aluminum-lithium alloy have higher welding porosity and thermal cracking susceptibility than traditional aluminum alloys. Therefore, it is difficult to weld aluminum-lithium alloys with lasers. On the contrary, laser swing welding can stir the molten pool to suppress the formation of welding defects and improve welding quality. The current research on double-sided laser welding of aluminum-lithium alloy T-joints mainly focuses on improving the welding quality by adjusting process parameters or improving the chemical composition of the welding wire but primarily for thin plates below 2 mm. In this study, we combine double-sided laser and laser swing welding technologies to realize double-sided laser swing welding of 2195-T87 aluminum-lithium alloy T-joint. As a result, we obtain a joint with better surface forming, lower porosity, and greater strength. We hope this study can be a reference for the engineering application of double-sided laser swing welding of 2195 aluminum-lithium alloy T-joints.

Methods 2195 aluminum-lithium alloy is used in this study. First, double-sided laser swing welding with circular swing method and traditional nonswing double-sided laser welding are used for welding 2195-T87 aluminum-lithium alloy T-joints with ER4047 Al-Si welding wire. Then, visual techniques are used to compare the surface formation of welds obtained by different welding methods and process parameters. After that, the X-ray nondestructive testing method is used to compare the porosity of welds completed by laser swing and nonswing welding. Next, the metallographic microscope is used to observe and compare the cross-sectional morphology of different welds, and scanning electron microscope (SEM) is used to examine the joints and contrast the structural characteristics with the joint structure obtained by other welding methods. In addition, the electronic universal testing machine is used to conduct transverse and axial tensile tests on the welds completed by laser swing and nonswing welding and then compare their transverse and axial tensile strengths. Finally, SEM is used to examine the samples' cross sections and analyze their fracture mode.

Results and Discussions The weld surface formed by double-sided laser swing welding is fuller and more uniform than that obtained by nonswing double-sided laser welding (Fig. 6). The internal porosity of the weld obtained by nonswing double-sided laser welding is significantly higher than that of the swing welding. Double-sided laser swing welding reduces the porosity from 1.89% of the weld obtained by the nonswing double-sided laser welding to 0.52% (Fig. 8). With the increase of welding speed, the weld's ripples gradually become more detailed and uniform, the quality of weld formation is improved, the penetration width is steadily reduced, and the thermal impact on the skin is reduced (Table 3). With the swing amplitude and frequency increase, the ripples on the weld's surface become finer, enhancing the surface shape. However, when the swing amplitude and frequency are too high, the weld's surface dramatically collapses, and when the swing amplitude is too high, the wall panel is not penetrated (Tables 4–5). Compared with nonswing double-sided laser welding, the average diameter of equiaxed crystals in the middle of the weld obtained by double-sided laser swing welding has been reduced from 21 to 13 μm (Fig. 10). In addition, the average diameter of the equiaxed fine-grained region has been reduced from 44 to 23 μm (Fig. 11). The joints obtained by double-sided laser swing welding have an axial tensile strength of 267 MPa and transverse tensile strength of 420 MPa, which increase by 123 MPa and 95 MPa, respectively, compared with nonswing welding (Fig. 12). Microporous aggregation fractures mainly characterize the fractures on the side of the welds. They have

intergranular and transgranular fracture characteristics. The fracture on the side of the base metal is a combination of quasi-cleavage and microporous aggregation fractures (Figs. 13–14).

Conclusions This study combines double-sided laser and laser swing welding technologies to realize a double-sided laser swing welding of 2195-T87 aluminum-lithium alloy T-joint. Double-sided laser swing welding with circular swing method is used to obtain 2195-T87 aluminum-lithium alloy T-joint with firm surface forming and low porosity. The porosity rate is reduced from 1.89% to 0.52%. Compared with conventional double-sided laser welding, double-sided laser swing welding can significantly refine the equiaxed crystal area in the middle of the weld by beam swinging and stirring the molten pool, and significantly reduce the size of the equiaxed, fine-crystal area to enhance the joint's load-bearing capacity. The average diameter of the equiaxed crystal in the middle is reduced from 21 to 13 μm , while the average diameter of the equiaxed, fine-crystal region is reduced from 44 to 23 μm . The obtained joints have maximum axial and transverse tensile strengths of 267 and 420 MPa, respectively. Compared with nonswing welding, they increased by 123 and 95 MPa, respectively, reaching 45% and 70% of the base metal strength. Our study shows that double-sided laser swing welding can design 2195-T87 aluminum-lithium alloy joints of better surface forming, lower porosity, and greater strength.

Key words laser technique; aluminum-lithium alloy T-joint; double-sided laser swing welding; microstructure; mechanical properties